ELSEVIER

Contents lists available at ScienceDirect

Applied Energy

journal homepage: www.elsevier.com/locate/apenergy



Improvement of H₂-rich gas production with tar abatement from pine wood conversion over bi-functional Ca₂Fe₂O₅ catalyst: Investigation of inner-looping redox reaction and promoting mechanisms



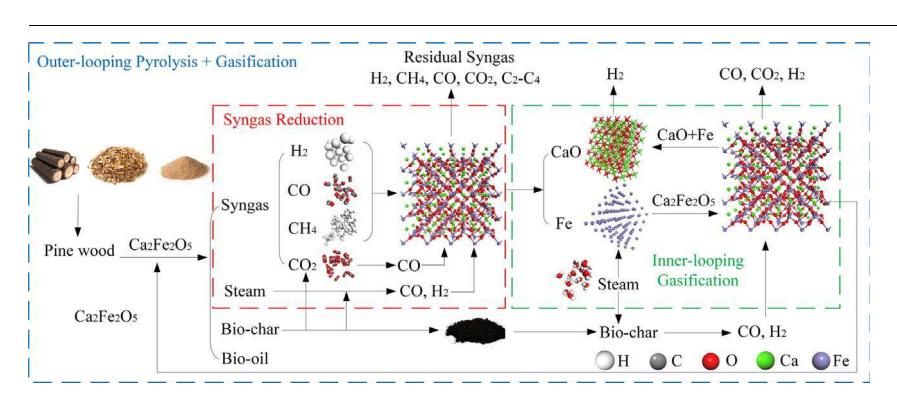
Zhao Sun^{a,b}, Shiyi Chen^a, Christopher K. Russell^c, Jun Hu^a, Asif H. Rony^b, Gang Tan^d, Aimin Chen^e, Lunbo Duan^a, John Boman^f, Jinke Tang^g, TeYu Chien^g, Maohong Fan^{b,h,i,*}, Wenguo Xiang^{a,*}

- a Key Laboratory of Energy Thermal Conversion and Control of Ministry of Education. School of Energy and Environment, Southeast University, Naniing 210096, China
- ^b Departments of Chemical and Petroleum Engineering, University of Wyoming, Laramie, WY 82071, USA
- ^c Department of Civil and Environmental Engineering, Stanford University, Stanford, CA 94305, USA
- d Department of Civil and Architectural Engineering, University of Wyoming, Laramie, WY 82071, USA
- ^e College of Chemical Engineering, Zhejiang University of Technology, Hangzhou 310023, China
- f Department of Criminal Justice, University of Wyoming, Laramie, WY 82071, USA
- ⁸ Departments of Physics & Astronomy, University of Wyoming, Laramie, WY 82071, USA
- ^h School of Energy Resources, University of Wyoming, Laramie, WY 82071, USA
- i School of Civil and Environmental Engineering, Georgia Institute of Technology, Atlanta, GA 30332, USA

HIGHLIGHTS

- A modified sol-gel method was used for the preparation of calcium ferrites.
- Ca₂Fe₂O₅ was found to facilitate tar abatement and biochar conversion.
- Ca plays an essential role in achieving steam oxidation from Fe⁰ to Fe³⁺.
- An inner-looping redox reaction and promoting mechanisms are proposed.

GRAPHICAL ABSTRACT



ARTICLE INFO

Keywords: Pine wood Hydrogen Catalytic Ca₂Fe₂O₅ Inner-looping

ABSTRACT

The objective of this research was to find cost-effective inner-looping redox-reaction-based biomass conversion catalysts by screening five Fe-containing materials through the integration of pine wood pyrolysis and gasification. All the evaluation tests are conducted in a fixed bed reactor under atmospheric pressure. The effect of temperature, water injection rate (steam/biomass ratio), catalyst loading, and reaction time on pine wood conversion performances was investigated. $Ca_2Fe_2O_5$ catalyst was found to facilitate H_2 -rich gas production, tar abatement, and carbon conversion. The maximum H_2 yield of 7.12 mol· H_2 /kg·Biomass was obtained in the first 10 min of gasification, which increased H_2 yield by 78.98% compared to biomass gasification under the water injection rate of 0.10 mL/min and catalyst load amount of 10 wt.% at 850 °C. Moreover, the hydrogen utilization, carbon conversion, and total gas yield of the process due to the use of $Ca_2Fe_2O_5$ increase by 13.4%, 17.3%, and

E-mail addresses: mfan@uwyo.edu, mfan3@mail.gatech.edu (M. Fan).

^{*} Corresponding authors at: Departments of Chemical and Petroleum Engineering, University of Wyoming, Laramie, WY 82071, USA (M. Fan); School of Energy and Environment, Southeast University, Nanjing 210096, China (W. Xiang).

11.7%, respectively. Continuous high yields of H_2 -enriched syngas were observed during the cyclic stability tests, indicating significant activity and redox durability of $Ca_2Fe_2O_5$. The catalyst characterization using BET, XRD, H_2 -TPR, SEM/EDS, and TEM revealed that $Ca_2Fe_2O_5$ is stable when tested cyclically, which results from the existence of Ca^{2+} in $Ca_2Fe_2O_5$. The bi-functional $Ca_2Fe_2O_5$ catalyst provides a novel way of inner-looping redox reaction for the continuous conversion of biomass.

1. Introduction

Industrialization has improved the living standards of modern society, which has resulted in a continuous increase in global energy demand over the last several decades [1]. Fossil fuels are the backbone of the energy resources but their negative effects on climate can no longer be neglected [1-3]. Therefore, it is highly desirable to use a renewable feedstock for producing environmentally friendly energies. On one hand, biomass is identified as a promising feedstock for green chemicals production with zero net carbon emissions, a low sulfur content, as well as globally available characteristics [4-6]. On the other hand, hydrogen is regarded as a clean and efficient energy carrier which is considered one of the most promising substitutes for fossil fuels [7-9]. The thermochemical conversion methods of biomass include combustion, liquefaction, pyrolysis, and gasification [10,11]. Recent studies also show the exciting potential of hydrogen generation with biomass [12,13]. Among them, steam biomass gasification represents a promising route for hydrogen-rich syngas production as it increases the heating value of yielded syngas with fast conversion kinetics [14,15]. However, low hydrogen yield and undesired high tar generation during gasification have stymied the large-scale application of the technology [16].

To cope with these challenges, catalysis has played an important role in the gasification process for inhibiting tar formation, accelerating biomass conversion, and enhancing the overall quantity and quality of syngas [16,17]. The presence of a catalyst during the biomass gasification process promotes several critical reactions such as secondary cracking and reforming, water gas shift, and hydrocarbon reforming, which improves the composition and heating value of the generated gases [18]. Several types of catalysts have been investigated to lower tar content in syngas for biomass gasification, including Ni- [14,19], Co- [18], and Fe-containing materials [20]. Although transition metal catalysts may exhibit excellent catalytic activity at relatively low temperatures, they are lacking in stability due to carbon deposition, sintering, and agglomeration [21,22]. Noble metal catalysts are also very helpful for biomass gasification, but their costs are unbearable in their industrial applications [23]. Calcium oxide (CaO) plays an important role in reforming tar and promoting carbon dioxide (CO₂) consumption [24,25]. CO₂ can be adsorbed by CaO, thereby shifting the water gas shift in the desired direction, and thus resulting in high hydrogen yield [26,27]. However, the activities of CaO decreased after several sorption-desorption cycles due to severe pore blockage and sintering and agglomeration. Moreover, a relatively large amount of CaO is required during the sorption-enhanced biomass gasification process to obtain a high concentration of H2 through CO2 sorption.

Recently, several metal composite oxides such as NiFe $_2O_4$, Ca $_2$ Fe $_2O_5$, CaFe $_2O_4$, LaFeO $_3$, and LaCeFeO $_3$ have attracted people's attention due to their excellent (hydro)thermal stability and low costs. Calcium ferrites have been proven to be environmentally safe, chemically stable, inexpensive, and abundant [28]. Huang et al. proved that the decrease in tar production is attributed to the synergy of CaO and Ca $_2$ Fe $_2$ O $_5$, which puts off the deactivation of CaO and promotes biomass gasification and H $_2$ production [29]. Ca $_2$ Fe $_2$ O $_5$ -Fe $_2$ O $_3$ catalyst was used by Zamboni et al. for hydrogen production from toluene steam reforming. Their results suggest that the activity of Fe/CaO depends on the stability of the interactions between iron and calcium under reaction conditions [30]. Ismail et al. synthesized a Ca-Fe based catalyst and demonstrated its additional capacity for hydrogen production through

chemical looping [31,32]. Researchers also demonstrated that a slight shift of the iron atoms from the cubic perovskite structure creates oxygen vacancies and facilitates the mobility of oxygen [33,34]. Moreover, these oxygen vacancies in $Ca_2Fe_2O_5$ provide the catalytic properties in deep oxidation of carbon monoxide, oxidation of volatile organic compounds, and in direct decomposition of NOx in exhaust steams [35–38]. Martin et al. demonstrated that CaO-containing Fe_2O_3 or $Ca_2Fe_2O_5$ produced more hydrogen from steam than pure Fe_2O_3 [39].

However, few studies have explored the possibility of H_2 enhancement and tar reduction with the actual biomass such as pine wood through the integration of pyrolysis and gasification by using the bifunctional $Ca_2Fe_2O_5$ catalyst. Thus, this research was designed to bridge the gap from the perspective of understanding the interaction among $Ca_2Fe_2O_5$, syngas, steam and biochar, and the catalytic promoting mechanisms in the catalytic pyrolysis and steam gasification. $Ca_2Fe_2O_5$ can be reduced by CO and H_2 resulting from steam biochar reaction for the generation of CaO and Fe, and oxidized by steam subsequently during steam gasification, a redox chemical looping according to the previous studies [30,39]. Thus, the inner-looping redox gasification represents chemical looping cycle through the reduction and oxidation reactions occurring in one reactor, while the outer-looping cycle denotes catalytic pyrolysis of biomass and inner-looping gasification of biochar.

In this study, three calcium ferrite catalysts ($CaO-Ca_2Fe_2O_5$, $Ca_2Fe_2O_5$, and $CaFe_2O_4$) were explored for converting pine wood and increasing H_2 -rich syngas yields with tar abatement with Fe_2O_3 and $FeCO_3$ being reference catalysts. The detailed objectives of this work are to (1) evaluate the effect of calcium ferrites in biomass pyrolysis and steam gasification processes on product yields and tar reduction performances; (2) explore the optimum operating conditions of pine wood gasification such as temperature, water injection rate, catalyst load content, and reaction time; (3) investigate the catalytic activity, cyclic stability, and phase evolution of the catalyst during biomass pyrolysis and steam gasification processes; and (4) analyze the continuous promoting mechanisms of the catalyst.

2. Methods

2.1. Materials

The beetle eroded pine wood, a kind of forestry waste in Wyoming of the U.S. was chosen to investigate catalytic pyrolysis and steam gasification experiments. The pine wood sample was crushed and sieved with particle sizes ranging from 125 to 150 μm . Then, the sample was dried at a temperature of 105 °C for 12 h. The ultimate analysis was determined by an elemental analyzer, as seen in Table 1. The mass concentrations of C, H, and O in the pine wood are 50.36%, 6.20%, and 43.06%, respectively. Thus, the H/C and O/C molar ratios of pine wood are 1.477 and 0.641, respectively, suggesting that the molecular formula of pine wood could be defined as $CH_{1.477}O_{0.641}$. The ash composition of pine wood samples was detected by using X-Ray Fluorescence (XRF) analysis as shown in Table 2.

2.2. Catalyst preparation and characterization

A modified citric acid assisted sol-gel method is used for calcium ferrite catalysts preparation, following the instructions previously

 Table 1

 Proximate and ultimate analysis of pine wood composition.

Fixed carbon	16.50
Volatile	78.12
Volutile	
Moisture	5.09
Ash	0.29
Ultimate analysis (% by weight,)
Carbon	50.36
Hydrogen	6.20
Nitrogen	0.33
Oxygen	43.06
Sulfur	0.05

Table 2Ash composition of pine wood samples using XRF analysis.

Compound	Biomass ash (%) 6.45	
SiO ₂		
Al_2O_3	1.93	
Fe_2O_3	2.54	
CaO	42.90	
MgO	13.61	
Na ₂ O	1.05	
K ₂ O	14.76	
MnO_2	3.58	
P_2O_5	2.69	
SrO	0.24	
BaO	0.18	
SO_3	1.63	

described [38]. In a typical experiment, Ca(NO₃)₂·4H₂O (Sigma-Aldrich No. 13477-34-4), Fe(NO₃)₃·9H₂O (Sigma-Aldrich No. 7782-61-8), and citric acid (Sigma-Aldrich No. 77-92-9) were mixed with desired molar ratios of Ca:Fe:citric acid = 2:1:6 for CaO-Ca₂Fe₂O₅ catalyst, Ca:Fe:citric acid = 1:1:4 for Ca₂Fe₂O₅ catalyst, and Ca:Fe:citric acid = 1:2:6 for CaFe₂O₄ catalyst. The mixture was then dissolved into a suitable amount of DI water, stirring constantly for 30 min at 40 °C. The solution was dried for 12 h at 180 °C. The product was crushed and sieved to suitable particle sizes and calcined in a furnace with a heating rate of 5 °C/min from room temperature to 850 °C and held for 4 h at atmospheric pressure.

X-ray diffraction (XRD) was conducted by a Rigaku Smartlab diffractometer by using Cu K α radiation source, operated at 40 kV and 40 mA with an angle of reflection, 20, varied between 20 and 80°. The Brunauer-Emmett-Teller (BET) surface areas were evaluated by an automatic Quantachrome instrument. All the samples were evacuated at

150 °C for 4h before adsorption. Temperature-programmed reduction (TPR) experiments were conducted in a quartz reactor equipped with an online mass spectrometer (Hiden, HPR-20 QIC) where 0.1 g of the sample was tested for each run. The sample was fluxed with helium gas to remove any other residual gases inside the reactor and on the surface of the sample at 150 °C for 30 min. When the catalyst was cooled down to 50 °C, a flow of 5% H₂ in N₂ was fed through the sample for 60 min. Then, the H₂-TPR experiment was carried out from 50 °C to 1050 °C at a heating rate of 5 °C/min under helium. Ca₂Fe₂O₅ catalyst was investigated by high-resolution transmission electron microscopy (HRTEM) using an FEI Tecnai G2 F20 S-Twin at 200 kV. It was first dispersed in ethanol under sonication treatment for 3 h. Then, the suspension was dropped onto a copper grid-supported transparent carbon foil and dried in the air for several minutes. The scanning electron microscopy (SEM) and energy dispersive spectrometer (EDS) were conducted using an FEI Quanta FEG 450 Scanning Electron Microscope with an acceleration voltage of 20 kV and spot size 4-7.

The thermal decomposition experiments were carried out using an SDT Q600 thermo gravimetric analyzer (TGA) with a heating rate of $10\,^{\circ}\text{C/min}$ and an N_2 flow rate of $100\,\text{mL/min}$ from room temperature to $900\,^{\circ}\text{C}$. The cyclic stability tests of $\text{Ca}_2\text{Fe}_2\text{O}_5$ were conducted using TGA in the alternate gas steam of $14.22\,\text{vol.}\%$ H_2 , $8.66\,\text{vol.}\%$ CH₄, $21.93\,\text{vol.}\%$ CO, $55.19\,\text{vol.}\%$ N_2 (for simulating catalytic pyrolysis) and $44.81\,\text{vol.}\%$ CO₂, $55.19\,\text{vol.}\%$ N_2 (for simulating gasification). The gas concentration is based on the gas production results during pyrolysis stage. The reduction syngas and the oxidation gas lasted for $10\,\text{min}$ and $5\,\text{min}$, respectively. To prevent the contact of the reduction and oxidation gas, $5\,\text{min}$ of N_2 purging process was conducted between each reactant gas switch.

2.3. Gasification

The pine wood steam gasification tests were carried out using a fixed bed reactor. The experimental devices primarily composed of an electrical furnace, a reactor, a steam generator, a temperature controller, a cold bath for tar collection, flow meters, and gas collecting bags as seen in Fig. 1. The reactor is made of a quartz tube with a length of 600.0 mm, an inner diameter of 10.0 mm, and an outer diameter of 12.8 mm. In a typical experiment, 2.0000 ± 0.0005 g of pine wood and 0.2000 ± 0.0002 g of catalyst were mixed together, followed by stirring and grinding constantly for at least 5 min. Then, the mixture was loaded into the constant temperature area of the quartz tube reactor. The system had been purged with N_2 before the furnace was heated from room temperature to a designed temperature (750 °C, 800 °C, 850 °C, or 900 °C) at the heating rate of 20 °C/min and N_2 flow rate of

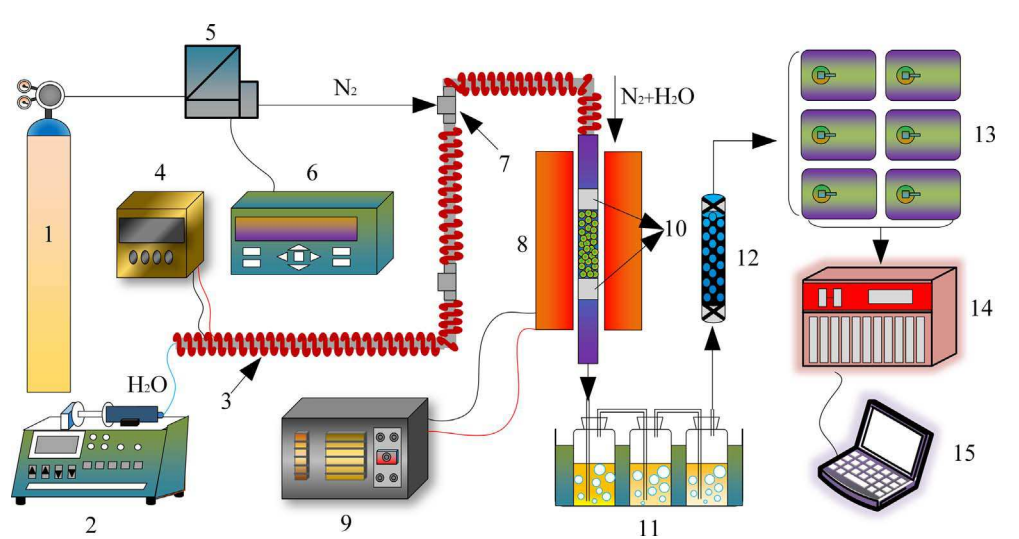


Fig. 1. Schematic diagram of fixed bed catalytic biomass outer-looping system. (1) N_2 cylinder; (2) HPLC pump, GenTech, 0.1– $10\,\mathrm{mL/min}$; (3) heating tape; (4) heating tape temperature controller; (5) mass flow meter, Parker 201, 0– $100\,\mathrm{mL/min}$; (6) mass flow controller, Parker CM-400; (7) three-way valve; (8) fixed bed furnace and quartz reactor, inner diameter of $1.2\,\mathrm{cm}$ length of $550.0\,\mathrm{mm}$; (9) temperature controller of furnace; (10) quartz wool; (11) ice bath; (12) moisture trap with dried CaSO₄ inside; (13) gas bags; (14) gas chromatograph, Inficon micro GC $3000\,\mathrm{and}$ SRI $8610\mathrm{C}$; (15) computer.

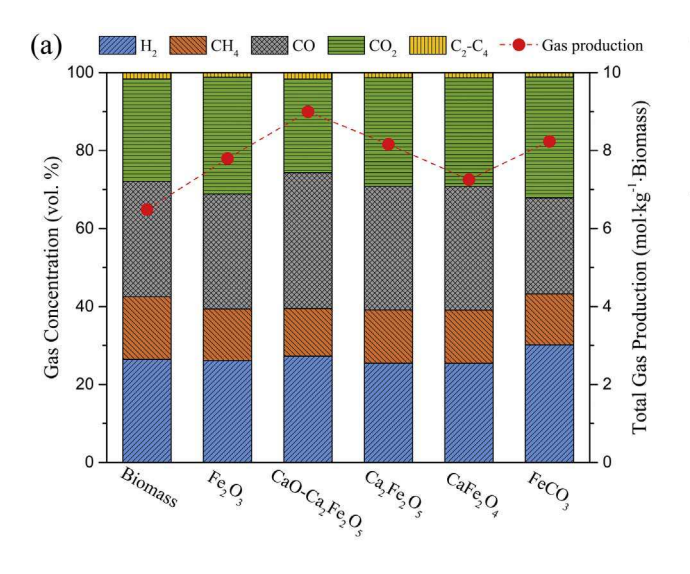
Table 3
Physical properties of Fe₂O₃, CaO-Ca₂Fe₂O₅, Ca₂Fe₂O₅, CaFe₂O₄, and FeCO₃ catalysts.

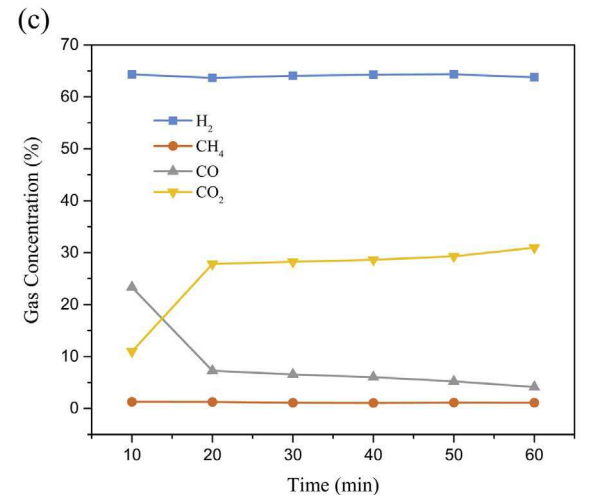
Catalyst	Crystal size (nm)	Average pore size (nm)	BET surface area (m²/g)	Pore volume (g/cm ³)
Fe ₂ O ₃	14.0	3.4	46.1	0.161
CaO-Ca ₂ Fe ₂ O ₅	19.0	3.1	45.2	0.060
$Ca_2Fe_2O_5$	23.1	3.1	67.1	0.066
CaFe ₂ O ₄	24.7	3.1	74.5	0.070
FeCO ₃	38.7	3.4	57.5	0.082

 $30\,mL/min.$ Once the specified temperature was reached, water was injected at the desired flow rate (0.02 mL/min, 0.06 mL/min, 0.10 mL/min, or 0.14 mL/min) by a syringe pump, and gasification stage proceeded. The produced gas was cleaned and dried and was then sampled with gas bags every 10 min. The concentrations of H_2 , CH_4 , CO, and CO_2 in each sample bag was determined by an INFICON 3000 Micro GC TCD detector, and the concentrations of $C_2\text{-}C_4$ are measured with a SRI 8610C GC FID detector.

2.4. Data analysis

The syngas component $(H_2, CH_4, CO, CO_2, and C_2-C_4)$ concentrations were calculated as follows:





$$C_{H_2} = \frac{C_{H_2,GC}}{C_{H_2,GC} + C_{CH_4,GC} + C_{CO_2,GC} + C_{C_2-C_4,GC}}$$
(E 1)

$$C_{CH_4} = \frac{C_{CH_4,GC}}{C_{H_2,GC} + C_{CH_4,GC} + C_{CO_2,GC} + C_{C_2-C_4,GC}}$$
(E 2)

$$C_{CO} = \frac{C_{CO,GC}}{C_{H_2,GC} + C_{CH_4,GC} + C_{CO,GC} + C_{CO_2,GC} + C_{C_2-C_4,GC}}$$
(E 3)

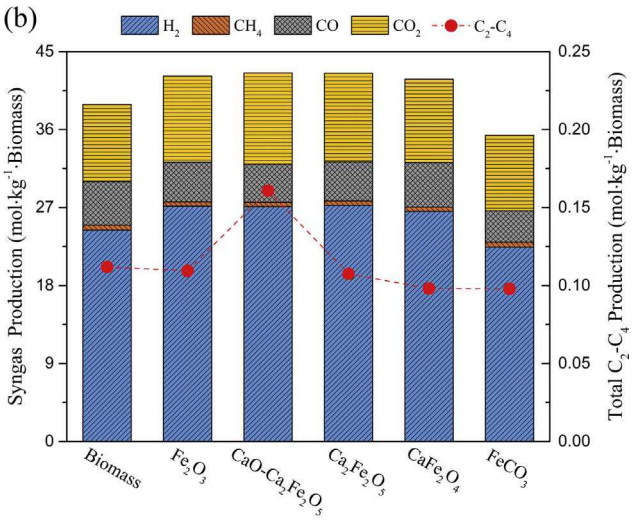
$$C_{CO_2} = \frac{C_{CO_2,GC}}{C_{H_2,GC} + C_{CH_4,GC} + C_{CO_2,GC} + C_{C_2-C_4,GC}}$$
(E 4)

$$C_{C_2-C_4} = \frac{C_{C_2-C_4,GC}}{C_{H_2,GC} + C_{CH_4,GC} + C_{CO_2,GC} + C_{C_2-C_4,GC}}$$
(E 5)

where $C_{H_2,C_{CH_4},C_{CO},C_{CO_2}}$, and $C_{C_2-C_4}$ represent the syngas concentrations of H_2 , CH_4 , CO, CO_2 , and C_2-C_4 , respectively, and $C_{H_2,G_C},C_{CH_4,G_C},C_{CO_2,G_C},C_{CO_2,G_C}$, and $C_{C_2-C_4,G_C}$ accordingly denote the concentrations of H_2 , CH_4 , CO, CO_2 , and C_2-C_4 calculated by CG. The total gas yields for one gas bag is calculated as:

$$Y_{\text{total,out}} = \frac{YR_{\text{N}_2,in} \times T}{C_{\text{N}_2,GC}}$$
 (E 6)

where $Y_{total,out}$ denotes the total gas yields from the gas sampling bag (Sigma 2L Tedlar PVDF), $YR_{N_2,in}$ is the flow rate of the inlet N_2 (30 mL/



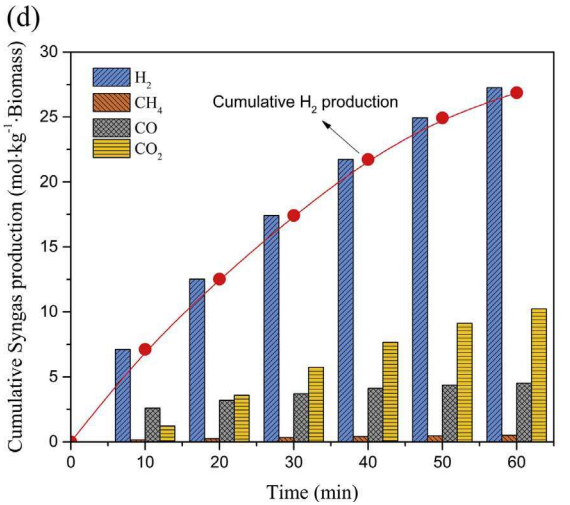


Fig. 2. Comparison of (a) gas composition and total gas production during pyrolysis stage, (b) syngas yields production during gasification stage and total C_2 - C_4 production during pyrolysis and steam gasification stages, (c) gas concentration at gasification stage using $C_{a2}Fe_2O_5$ catalyst, and (d) cumulative syngas production performances of the prepared catalysts. (N₂ flow rate: 30 mL/min, water injection rate: 0.10 mL/min, catalyst concentration: 10 wt.%, gasification time: 60 min, temperature: 850 °C).

 Table 4

 Carbon conversion of iron-containing catalysts during pyrolysis and steam gasification.

Catalysts	Carbon conversion (%)	
Pure biomass	84.53	
Fe ₂ O ₃	93.29	
CaO + Ca ₂ Fe ₂ O ₅	98.11	
Ca ₂ Fe ₂ O ₅	99.14	
CaFe ₂ O ₄	99.70	
FeCO ₃	91.95	

min), T is the N_2 flow time for each gas bag collection, and $C_{N_2,GC}$ represents the N_2 concentration of the gas bag calculated by GC. The hydrogen yields for one gas bag is calculated in the way of:

$$Y_{H_2,out} = Y_{total,out} \times C_{H_2,GC} \tag{E 7}$$

The cumulative H_2 yield is the sum of H_2 obtained with every 10 min:

$$Y_{sum,H_2,out} = \sum_{1}^{n} Y_{i,H_2,out}$$
 (n= 1,2,3,4,5,6) (E 8)

where $Y_{i,H_2,out}$ is the H_2 collected with No. i gas bag and $Y_{sum,H_2,out}$ represents the cumulative hydrogen yield. The carbon conversion, H_2/CO molar ratio, CO/CO_2 molar ratio, and hydrogen utilization are defined as:

Carbon conversion (%) =
$$1 - \frac{Carbon\ mass\ of\ residue\ after\ reaction}{Carbon\ mass\ of\ pine\ wood\ before\ reaction} \times 100\%$$
 (E 9)

$$H_2/CO$$
 molar ratio = $\frac{\text{Moles of } H_2 \text{ product}}{\text{Moles of CO product}}$ (E 10)

$$CO/CO_2$$
 molar ratio = $\frac{Moles \text{ of } CO \text{ product}}{Moles \text{ of } CO_2 \text{ product}}$ (E 11)

Hydrogen utilization (%)

$$= \frac{Hydrogen \text{yields production}}{Hydrogen \text{provided by steam+hydrogen in pine wood}} \times 100\%$$
(E 12)

3. Results and discussion

3.1. Catalyst screening

Five different iron-containing catalysts, Fe₂O₃, CaO-Ca₂Fe₂O₅, Ca₂Fe₂O₅, CaFe₂O₄, and FeCO₃, were tested to study their catalytic activity in the pyrolysis and steam gasification tests under the conditions of N2 flow rate 30 mL/min, catalyst loading 10 wt.%, water injection rate 0.10 mL/min, and gasification temperature at 850 °C. The physical properties of Fe₂O₃, CaO-Ca₂Fe₂O₅, Ca₂Fe₂O₅, CaFe₂O₄, and FeCO₃ catalysts are presented in Table 3 (see Figs. S1 and S2). The BET surface areas of Fe₂O₃, CaO-Ca₂Fe₂O₅, Ca₂Fe₂O₅, CaFe₂O₄, and FeCO₃ catalysts were $46.1 \text{ m}^2/\text{g}$, $45.2 \text{ m}^2/\text{g}$, $67.1 \text{ m}^2/\text{g}$, $75.4 \text{ m}^2/\text{g}$, and 57.5 m²/g, respectively. Moreover, the BET surface areas and pore volumes of sol-gel prepared CaO-Ca₂Fe₂O₅, Ca₂Fe₂O₅, and CaFe₂O₄ catalysts increase with the Fe/Ca molar ratio increasing and follows the trend of $CaFe_2O_4 > Ca_2Fe_2O_5 > CaO-Ca_2Fe_2O_5$. The thermos-decomposition properties and H2-TPR results of the catalysts were provided in the supplementary materials (see Figs. S3 and S4). The H₂-TPR results suggest that the reduction of CaO-Ca₂Fe₂O₅ or Ca₂Fe₂O₅ to Fe⁰ is complete in one step at a relatively high temperature and it is also proved by XRD results. However, the H2-TPR profile of CaFe2O4 is similar to Fe₂O₃ which performs three reduction peaks. The three reduction peaks can be attributed to the successive reduction of Fe3+ $(Fe^{3+} \text{ to } Fe^{2.67+}, Fe^{2.67+} \text{ to } Fe^{2+}, Fe^{2+} \text{ to } Fe^{0}).$

As seen in Fig. 2a, the CH₄ content in the syngas is reduced with the application of the five Fe-containing catalysts in the pyrolysis stage. The CO₂ content shows an obvious decrease for the tests with the application of CaO-Ca₂Fe₂O₅. The highest syngas production can be generated due to the existence of CaO for tar cracking and CO2 absorption. Furthermore, the total gas yields are in the order of CaO- $Ca_2Fe_2O_5 > FeCO_3 > Ca_2Fe_2O_5 > Fe_2O_3 > CaFe_2O_4 > pure$ mass. As can be seen in Fig. 2b, Fe₂O₃, CaO-Ca₂Fe₂O₅, Ca₂Fe₂O₅, and CaFe₂O₄ catalysts enhance syngas production, especially for CaO-Ca₂Fe₂O₅ and Ca₂Fe₂O₅ catalysts, whose syngas yields are 3.66 and 3.62 mol·kg⁻¹·biomass higher than pure biomass. However, the C₂-C₄ yields by using CaO-Ca₂Fe₂O₅ are much higher than other catalysts or pure biomass. The phenomenon can be explained that heavier hydrocarbons were converted to light hydrocarbons due to the cracking effect of CaO. The carbon conversion during biomass pyrolysis and steam gasification with and without catalysts are shown in Table 4. The highest carbon conversion of 99.70% is obtained by using CaFe₂O₄ catalyst followed by the conversion of 99.14% with Ca₂Fe₂O₅ catalyst. These results indicate that the biomass is converted into more syngas or bio-oil through the pyrolysis and steam gasification with Fe-based

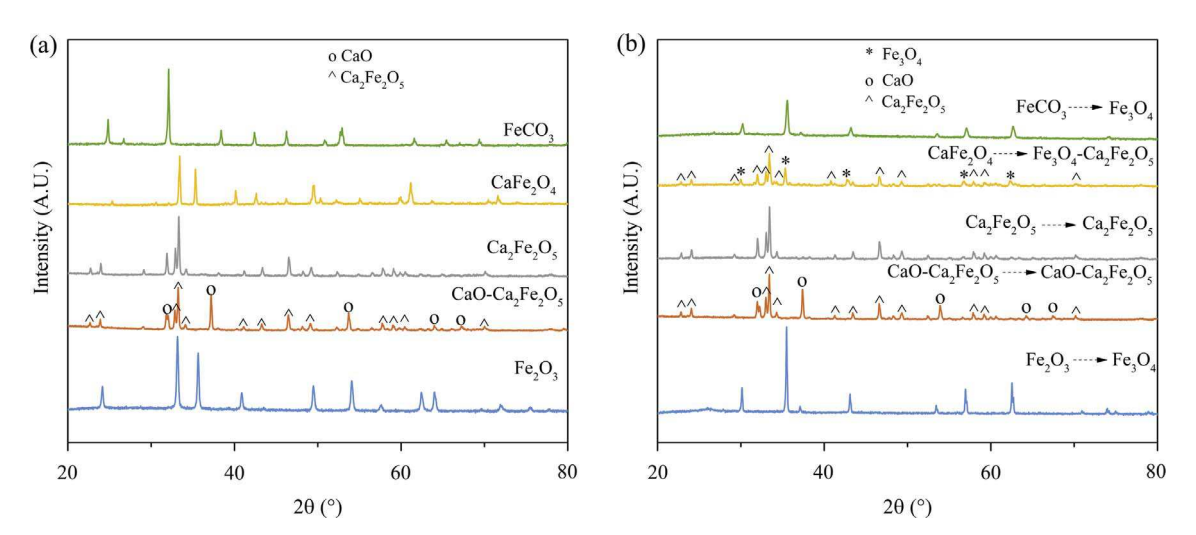


Fig. 3. XRD analysis of the (a) fresh catalysts and (b) reacted catalysts.

catalysts. The syngas concentration and cumulative production in the steam gasification stage with $\text{Ca}_2\text{Fe}_2\text{O}_5$ catalyst were displayed as seen in Fig. 2c and Fig. 2d. The syngas is mainly composed of H_2 , CO, and CO_2 gas with little CH_4 generation. The detailed information regarding gas concentration and production for all the catalysts were provided in Fig. S5. As can be seen, the H_2 production rate is relatively high for the first 20 min of biomass gasification. Thus, the cumulative H_2 yields production with applied different catalysts are analyzed and compared to further clarify the performances of catalytic biomass gasification (see Fig. S6). It is obvious that the H_2 yields improved a lot with the addition of Fe-containing catalysts, especially for Fe_2O_3 , $\text{CaO-Ca}_2\text{Fe}_2\text{O}_5$, $\text{Ca}_2\text{Fe}_2\text{O}_5$, and CaFe_2O_4 catalysts.

Analysis of the fresh iron-containing catalysts reveals that the dominant X-ray diffraction spectrum is fitted with Fe₂O₃ (PDF card number 99-0060), CaO-Ca₂Fe₂O₅ (99-0070 and 71-2264), Ca₂Fe₂O₅ (71-2264), CaFe₂O₄ (72-1199), and FeCO₃ (83-1764), respectively (see Fig. 3a). Fig. 3b represents the reacted Fe₂O₃, CaO-Ca₂Fe₂O₅, Ca₂Fe₂O₅, CaFe₂O₄, and FeCO₃ catalysts after the pyrolysis and steam gasification stages. As can be seen, the XRD phases of reacted Fe₂O₃, CaFe₂O₄, and FeCO₃ catalysts are reproduced to be Fe₃O₄ (89-0688), Ca₂Fe₂O₅-Fe₃O₄ (71-2264 and 89-0688), and Fe₃O₄ (75-0033) respectively after steam gasification which indicates that the Fe₂O₃, CaFe₂O₄, and FeCO₃ catalysts could not be restored automatically. As for reacted CaO-Ca₂Fe₂O₅ and Ca₂Fe₂O₅ catalysts, their phases are stable and remain CaO-Ca₂Fe₂O₅ (99-0070 and 71-2264) and Ca₂Fe₂O₅ (71-2264), respectively.

The XRD results demonstrate that the fresh Ca₂Fe₂O₅ and CaO-Ca₂Fe₂O₅ catalysts maintain their original phase after 60 min of steam gasification at 850 °C. The syngas reduced catalyst (Fe⁰) was completely oxidized to Fe³⁺ in the presence of CaO. For Fe₂O₃ and FeCO₃ catalysts, Fe₃O₄ is the final product after catalytic pyrolysis and steam gasification, which indicates an incomplete oxidation after steam gasification process. For CaFe₂O₄ catalyst, the syngas reduced catalyst (Fe⁰) would partially combine with CaO and form Ca₂Fe₂O₅, indicating Ca₂Fe₂O₅ is a more stable phase than the other calcium ferrites; another part of syngas reduced catalyst without CaO combination could not be completely oxidized by steam, and thus Fe₃O₄ is formed instead. One of the most important requirements for catalyst selection is whether the catalyst is both active and regenerative [40]. From this point of view, CaO-Ca₂Fe₂O₅ and Ca₂Fe₂O₅ were seen as promising catalysts for biomass conversion. Ca₂Fe₂O₅ was chosen for further investigation due to its catalytic activity, automatic regeneration, and high carbon conversion.

The TEM micrographs of $Ca_2Fe_2O_5$ catalyst are shown in Fig. 4. An irregular spherical-like structure is observed. The results indicate a relatively uniform distribution of particle sizes. Moreover, according to the XRD results the catalyst mainly consists of $Ca_2Fe_2O_5$. Thus, the dark spots are inferred to be the crystal cross and overlap. Moreover, it can

be seen that the particle sizes of $Ca_2Fe_2O_5$ are ranged from 20 to 30 nm. The Scherrer equation results indicate the representative crystal size of the fresh $Ca_2Fe_2O_5$ is 23.1 nm which is consistent with the results observed with TEM.

3.2. Effect of temperature and water injection rate

As can be seen from Fig. 5a, the total gas production increases gradually with the gasification temperature. The concentrations of H2 and CO increase with temperature, while the concentrations of CH₄ and CO2 decreases with temperature. Carbon dioxide reforming of CH4 as well as the Boudouard reaction can be enhanced by increasing temperature, leading to the increases in the concentrations of H₂ and CO as well as the syngas yield. Both temperature and water injection rate considerably affect hydrogen production as shown Fig. 5b, Fig. 5c, and Fig. 5d. The integration of varied temperature and water injection rate leads to a relatively uniform increase in hydrogen production during gasification. The hydrogen generation rate decreases with time, the trend elevates with the proceeding of gasification, which is very obvious within 20-60 min. H₂ yield at 850 °C provided in Fig. 5d is slightly higher than that of 900 °C with water injection rates varying from 0.06 to 0.10 mL/min. This results from the increase in temperature and thus biochar conversion in the pyrolysis stage. The less amount of biochar remains for the gasification stage certainly leads to lower production of H2.

As can be seen from Fig. 6a, the total gas production performs similar distribution to the hydrogen production at 60 min. 850 °C is seen as a suitable gasification temperature for maximum gas yield. The total gas production reaches the highest of 44.2 mol·kg⁻¹·Biomass with the water injection rate of 0.14 mL/min at 850 °C (see Fig. 6b). Carbon conversion is close to 100% when the temperatures are higher than 850 °C and the water injection rates are higher than 0.10 mL/min. Increasing the water injection rate led to higher H2/CO molar ratios under the same temperature (see Fig. 6c and Fig. 6d). Raising the water injection rate promotes the water gas reaction, which produces more CO and H2. The produced CO gas would react with Ca2Fe2O5 further and produce more CO₂ gas. Thus, the H₂/CO and CO/CO₂ ratios perform the tendency of increasing and decreasing, respectively, as the water injection rate increased. Furthermore, a high water injection rate promotes the Fe⁰ oxidation reaction and thus accelerates the reaction process. It is also seen that the H₂/CO molar ratios decrease with temperature under the same water injection rate. This could be explained by (1) The limited amount of catalyst loading. The rise of temperature would promote the primary steam biochar reaction and generate more CO and H2. The produced CO gas could not be fully oxidized by the limited amount of catalyst loading; (2) The Boudouard reaction is promoted due to the temperature rise which regenerates

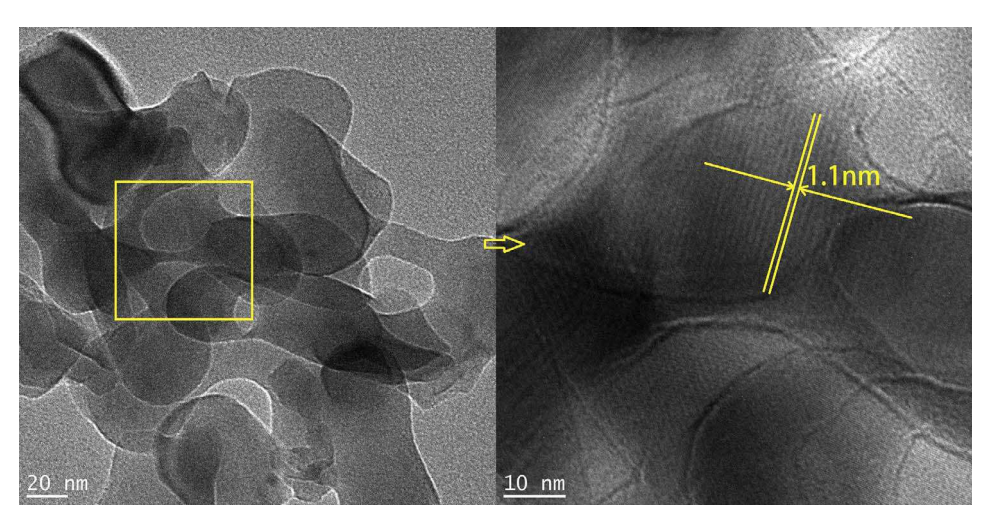


Fig. 4. TEM images for the fresh Ca₂Fe₂O₅ catalyst.

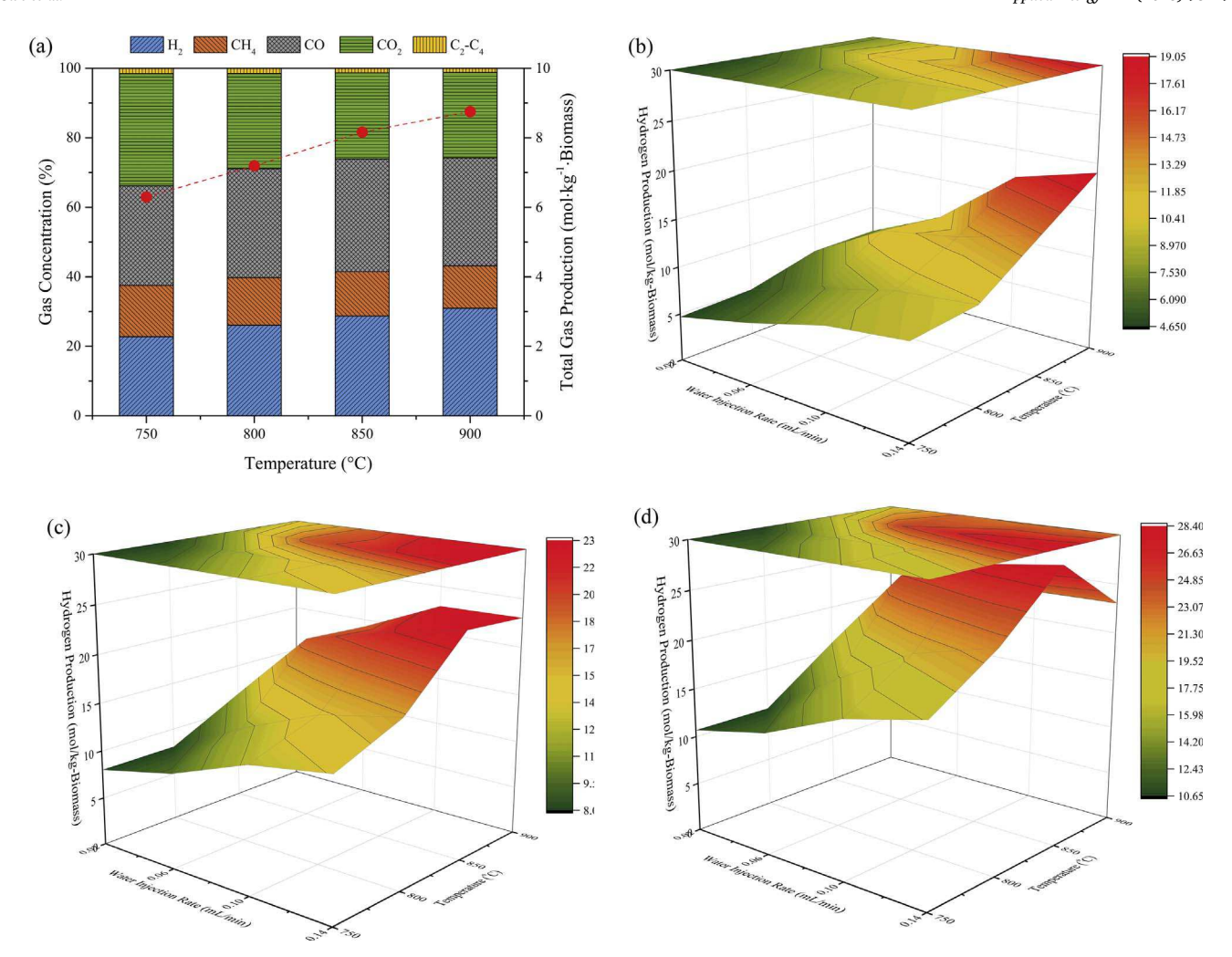


Fig. 5. Effect of temperatures (750 °C, 800 °C, 850 °C, and 900 °C) and water injection rates (0.02 mL/min, 0.06 mL/min, 0.10 mL/min, and 0.14 mL/min) on syngas/hydrogen production during the (a) pyrolysis stage, (b) gasification stages after 20 min, (c) 40 min, and (d) 60 min (N₂ flow rate: 30 mL/min, catalyst concentration: 10 wt.% Ca₂Fe₂O₅).

more CO.

3.3. Effect of catalyst content

As can be seen from Fig. 7a, the total syngas yields increased from 6.5 to $8.7\,\mathrm{mol\cdot kg^{-1}\cdot Biomass}$ as the catalyst concentration increased from 0 to 15 wt.% Ca₂Fe₂O₅ during catalytic pyrolysis. More CO₂ and H₂O can be generated due to the increase in Ca₂Fe₂O₅ loading and subsequently promote the tar conversion. The CH₄ concentration decreased from 16.0 vol.% to 13.5 vol.%, 12.5 vol.%, and 11.9 vol.% with the catalyst addition from 0 to 5 wt.%, 10 wt.%, and 15 wt.%, respectively. The results reveal that the addition of catalyst has an effect on methane, and the more the Ca₂Fe₂O₅ catalysts are loaded, the lower the methane content. On one hand, more produced syngas could be oxidized by with the addition of Ca₂Fe₂O₅ including CH₄; on the other hand, the generation of H₂O and CO₂ could also promote the conversion of CH₄. Similarly, as the catalyst concentration increased, the C₂-C₄ concentrations decrease gradually from 1.7 vol.% to 1.5 vol.%, 1.3 vol. %, and 1.1 vol.%, respectively. Moreover, the concentration of CO performs obvious increasing trend with the Ca₂Fe₂O₅ concentration, which could be attributed to the partial oxidation of syngas with Ca₂Fe₂O₅ or the regeneration of CO from Boudouard reaction.

As shown in Fig. 7b, the addition of $Ca_2Fe_2O_5$ to 10 wt.% produced the highest syngas yields of 42.5 mol·kg⁻¹·Biomass and the syngas production follows the trend of 10 wt.% > 15 wt.% > 5 wt.% > 0 wt.%. It could be explained that more biomass is converted to oil or syngas

with the $Ca_2Fe_2O_5$ loading increasing from 10 wt.% to 15 wt.% at the pyrolysis stage, resulting in a less provision of biochar and lower total gas production for the 15 wt.% catalyst loading during steam gasification. The cumulative H_2 and CO production at first 30 min are both in the order of 15 wt.% > 10 wt.% > 5 wt.% > 0 wt.% but only slightly change as the gasification time increases from 30 min to 60 min with the catalyst loading (see Fig. 7c and Fig. 7d). Thus, the $Ca_2Fe_2O_5$ load content affects the products distribution in the gasification stage. Higher concentration of the catalyst would result in higher CO and H_2 production and thus improve the quality of gas products.

3.4. Cyclic stability of Ca₂Fe₂O₅

It could be found from Fig. 8a that the syngas (H_2 , CH_4 , CO, CO_2 , and C_2 - C_4) concentration is relatively stable within the first 5 cycles. The total gas production during the pyrolysis stage is slightly reduced after 4th cycles. The total syngas yield including C_2 - C_4 also maintains stable, indicating the significant cyclic durability of the $Ca_2Fe_2O_5$ within the first 5 cycles (see Fig. 8b). And the H_2 production from 1st to 5th cycle is 26.5, 25.8, 26.5, 26.1, and 26.1 mol·kg $^{-1}$ ·Biomass, respectively. The cumulative H_2 and CO production are presented in Fig. 8c. The CO production rate decreases gradually with the gasification time, owing to the continuous oxidation of CO with $Ca_2Fe_2O_5$. The reduced Fe^{3+} (Fe^{0}) would re-oxidized by steam and generate H_2 constantly until the biochar is fully converted, thus a relatively high increasing rate of H_2 production is observed compared with CO. 20 cyclic

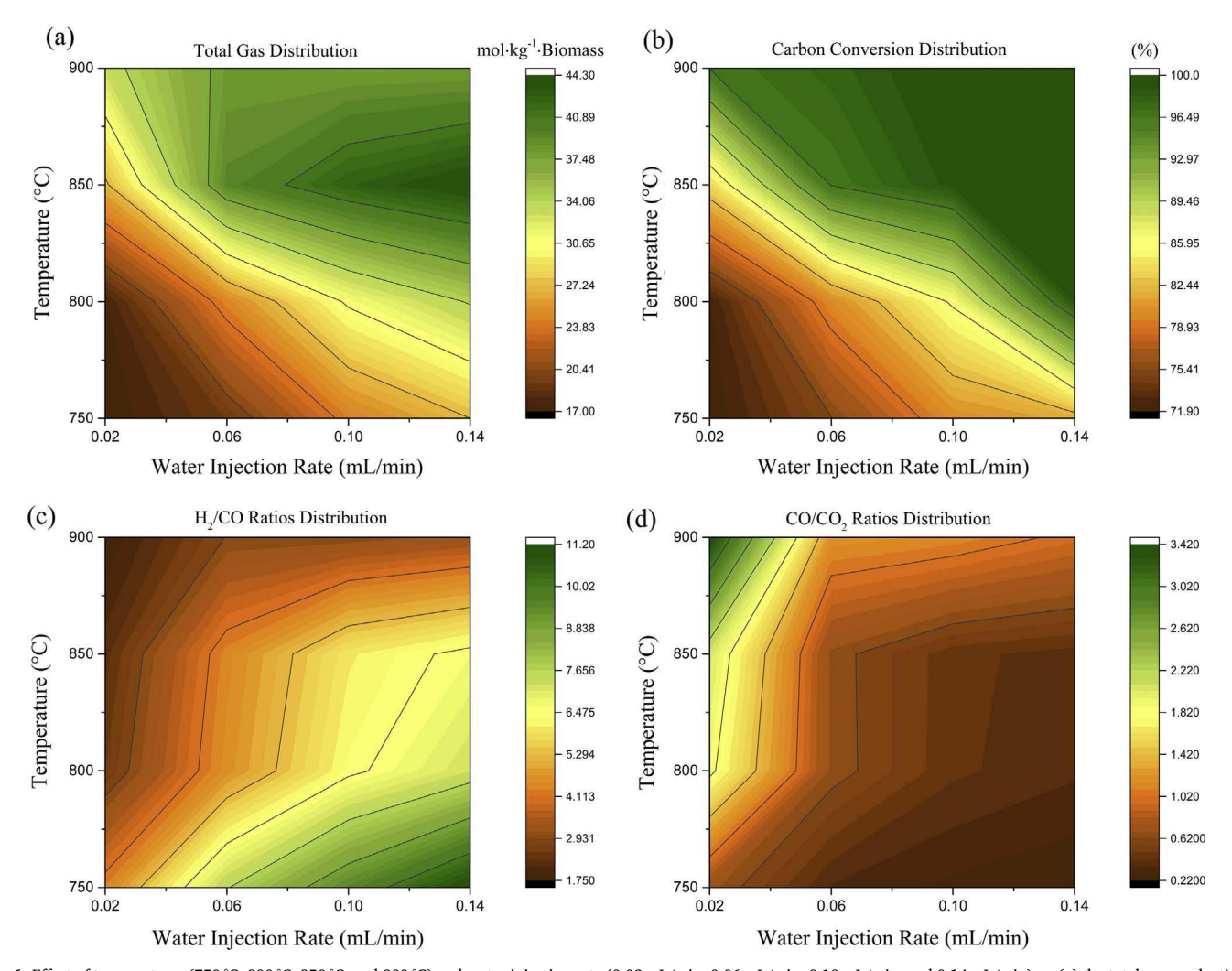


Fig. 6. Effect of temperatures (750 °C, 800 °C, 850 °C, and 900 °C) and water injection rate (0.02 mL/min, 0.06 mL/min, 0.10 mL/min, and 0.14 mL/min) on (a) the total gas production, (b) carbon conversion distribution, (c) H_2/CO ratios distribution, and (d) CO/CO_2 ratios distribution during the gasification process (N_2 flow rate: 30 mL/min, catalyst concentration: 10 wt.% $Ca_2Fe_2O_5$, gasification time: 60 min).

redox tests were carried out to further investigate the durability of the $\text{Ca}_2\text{Fe}_2\text{O}_5$ by using TGA with simulated syngas (21.93 vol.% CO + 8.66 vol.% CH₄ + 14.22 vol.% H₂) reduction and 44.81 vol.% CO₂ oxidation. Results indicate that the catalysts perform significant redox stability within 20 cycles (see Fig. 8d).

The effect of reaction time on the H₂/CO molar ratio, hydrogen utilization, carbon conversion, and catalyst phase evolution by using Ca₂Fe₂O₅ catalyst is presented in Fig. 9. The H₂/CO molar ratios of the syngas become higher with reaction time for both with and without catalyst loading. Moreover, the H2/CO ratio with Ca2Fe2O5 is higher compared with biomass gasification without catalyst loading after 10 min (see Fig. 9a). It is inferred that the higher the conversion of biochar during gasification, the higher the H₂/CO can be obtained due to the enhancement of secondary steam biochar reaction and water gas shift. As can be seen from Fig. 9b and c, the H2 utilization and the carbon conversion were found decreasing and increasing, respectively with the rise of gasification time. The decrease of hydrogen utilization with gasification time was found to be correlated with the increase of carbon conversion. The unreacted biochar decreased with time gradually while the amount of water injection rate keeps unchanged, leading to a decreasing of hydrogen utilization.

The XRD tests were carried out to detect the phase change of the $Ca_2Fe_2O_5$ catalyst at different gasification times (0 min, 20 min, 40 min, and 60 min) as shown in Fig. 9d. Results illustrate that CaO, Fe, and carbon are the main initial components and $Ca_2Fe_2O_5$ is the main

component after 20, 40, and 60 min of gasification, suggesting that the Fe-based catalyst could be oxidized by steam from ${\rm Fe^0}$ to ${\rm Fe^3}^+$ with the addition of CaO and remains in the phase of ${\rm Ca_2Fe_2O_5}$ during the whole gasification stage. Moreover, the peak intensity of XRD increased with the rise of gasification time, indicating higher crystallinity and stability of ${\rm Ca_2Fe_2O_5}$.

Fig. 10 shows the SEM images of a) fresh $Ca_2Fe_2O_5$ catalyst and b) reacted $Ca_2Fe_2O_5$ catalyst after 1st cycle of the outer-looping test (catalytic pyrolysis + steam gasification). As can be seen, the particles of reacted $Ca_2Fe_2O_5$ still maintain specific particle with a spherical-like shape. Some particles observed are larger than the fresh $Ca_2Fe_2O_5$ sample, which is attributed to the partial agglomeration and sintering of $Ca_2Fe_2O_5$ particles. The EDS mapping tests were also carried out to detect the $Ca_2Fe_2O_5$ particles. The EDS mapping tests were also carried out to detect the $Ca_2Fe_2O_5$ particles. The EDS mapping sets were also carried out to detect the $Ca_2Fe_2O_5$ particles. The EDS mapping tests were also carried out to detect the $Ca_2Fe_2O_5$ particles. The EDS mapping also proved the reacted sample. Moreover, the EDS mapping also proved the existence of unreacted carbon. The biochar is not deposited on the $Ca_2Fe_2O_5$ catalyst but was existed in the form of bulk together with the reacted $Ca_2Fe_2O_5$ catalyst.

3.5. Discussion

3.5.1. Syngas reduction

The outer-looping process (biomass pyrolysis and steam

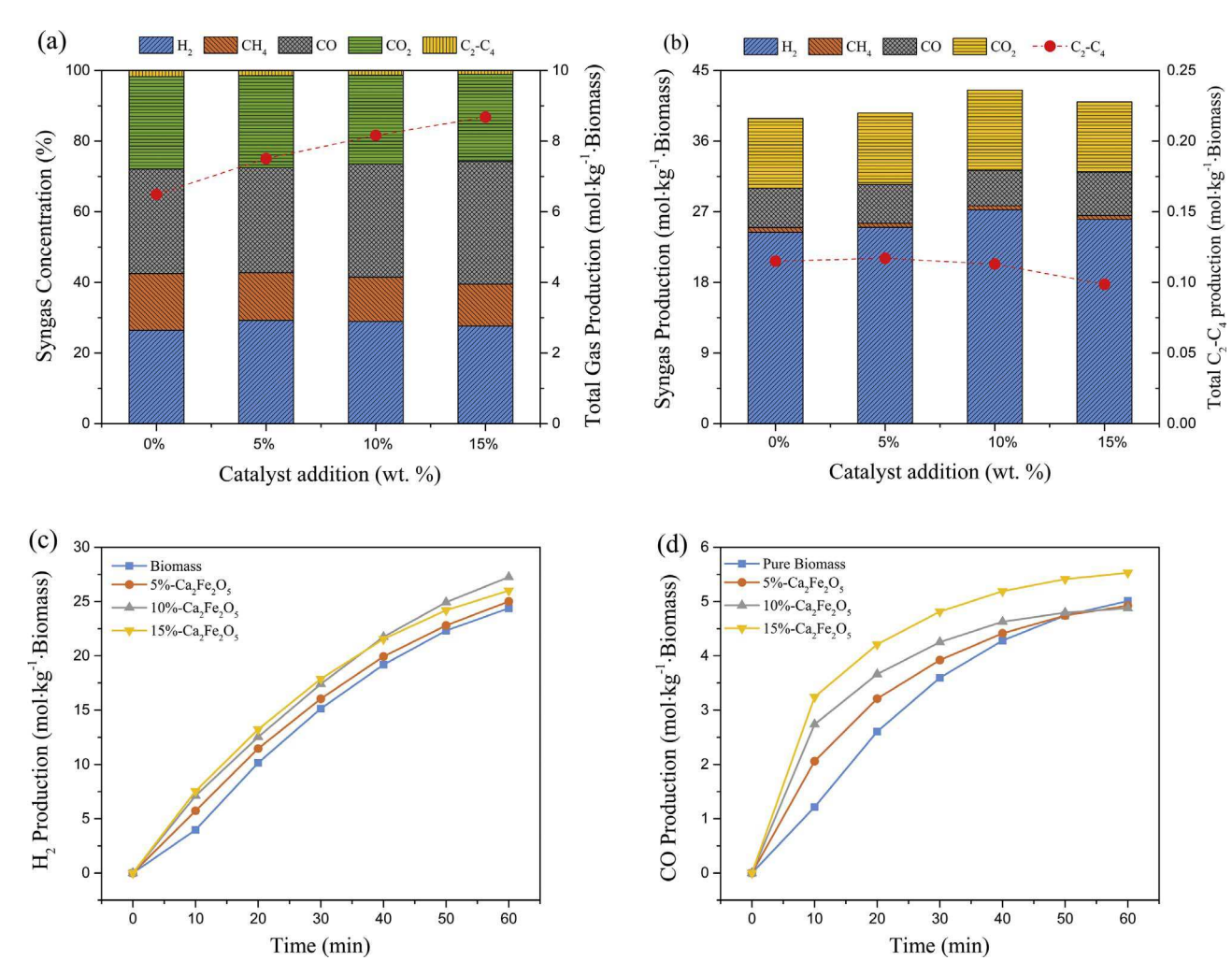


Fig. 7. Effect of $Ca_2Fe_2O_5$ concentration (0 wt.%, 5 wt.%, 10 wt.%, and 15 wt.%) on (a) gas composition and production during pyrolysis, (b) syngas yield during gasification, (c) cumulative H_2 production, and (d) cumulative CO production (N_2 flow rate: 30 mL/min, water injection rate: 0.10 mL/min, temperature: 850 °C, gasification time: 60 min).

gasification) in this study could be divided into two main stages: (1) pyrolysis, where biomass is decomposed into char, tar, and volatiles and the catalyst was reduced by the generated syngas; (2) steam reformation, where the catalyst was oxidized by steam, yielding regenerated catalyst and syngas [41,42]. The reactions at pyrolysis stage during thermos-chemical conversion pine wood using $Ca_2Fe_2O_5$ catalyst is concluded as follows:

Pyrolysis of pinewood proceeds in the ways of:

initiation:
$$CH_{1.477}O_{0.641} \rightarrow (H_2 + CO + CO_2 + CH_4 + C_2 + ...) + Tar + Char$$
 (R1)

tar cracking:
$$C_n H_m \rightarrow (m/2) H_2 + nC$$
 (R2)

 $Ca_2Fe_2O_5$ reduction with CO: $Ca_2Fe_2O_5 + 3CO \rightarrow 2CaO + 2Fe + 3CO_2$ (R3)

 $Ca_2Fe_2O_5$ reduction with H_2 : $Ca_2Fe_2O_5 + 3H_2 \rightarrow 2CaO + 2Fe + 3H_2O$ (R4)

tar conversion with
$$CO_2$$
: $C_nH_m(tar) + nCO_2 \rightarrow nCO + m/2H_2$ (R6)

tar conversion with H₂O:
$$C_nH_m(tar) + nH_2 O \rightarrow nCO + \left(\frac{m}{2} + n\right)H_2$$
 (R7)

As seen in (R1)–(R7), the reaction path becomes complicated with the addition of the $Ca_2Fe_2O_5$ catalyst. The $Ca_2Fe_2O_5$ catalyst is reduced by the produced syngas with the generation of H_2O and CO_2 during the pyrolysis stage. The produced tar can be decomposed to smaller molecular weight gases in the presence of H_2O and CO_2 . Although the addition of the $Ca_2Fe_2O_5$ catalyst consumes a portion of the reducing gas (H_2 , CO, and CO, the production of CO and CO further promotes the generation of syngas from tar conversion. The final products of biomass pyrolysis would be determined by the interaction of a couple of reactions mentioned above. It is known that the syngas produced in pyrolysis stage is mainly reductive atmosphere. Thus, the $Ca_2Fe_2O_5$ catalyst is displayed in the formation of reduction valence of Ca_2 indicating the generation of Ca_2 0 simultaneously as seen in reaction (R3)–(R5). The generation of Ca_2 0 would also enhance tar cracking and promote the biomass conversion during the pyrolysis stage.

3.5.2. Steam oxidation and inner-looping promotion

In the second gasification stage, steam was fed into the reactor which involves reactions of CO, $\rm H_2$, CO₂, CH₄, hydrocarbon gases with vapor, biochar, and the reduced $\rm Ca_2Fe_2O_5$ catalyst [15,20]. The main reactions were shown as follows:

steam oxidation of Fe⁰: 2Fe + 2CaO + 3H₂ O
$$\rightarrow$$
 Ca₂Fe₂O₅ + 3H₂ (R8)

steam tar reforming:
$$C_nH_m + 2nH_2 O \rightarrow \left(n + \frac{m}{2}\right)H_2 + nCO_2$$
 (R9)

steam biochar reaction (primary):
$$C+ H_2 O \rightarrow CO + H_2$$
 (R10)

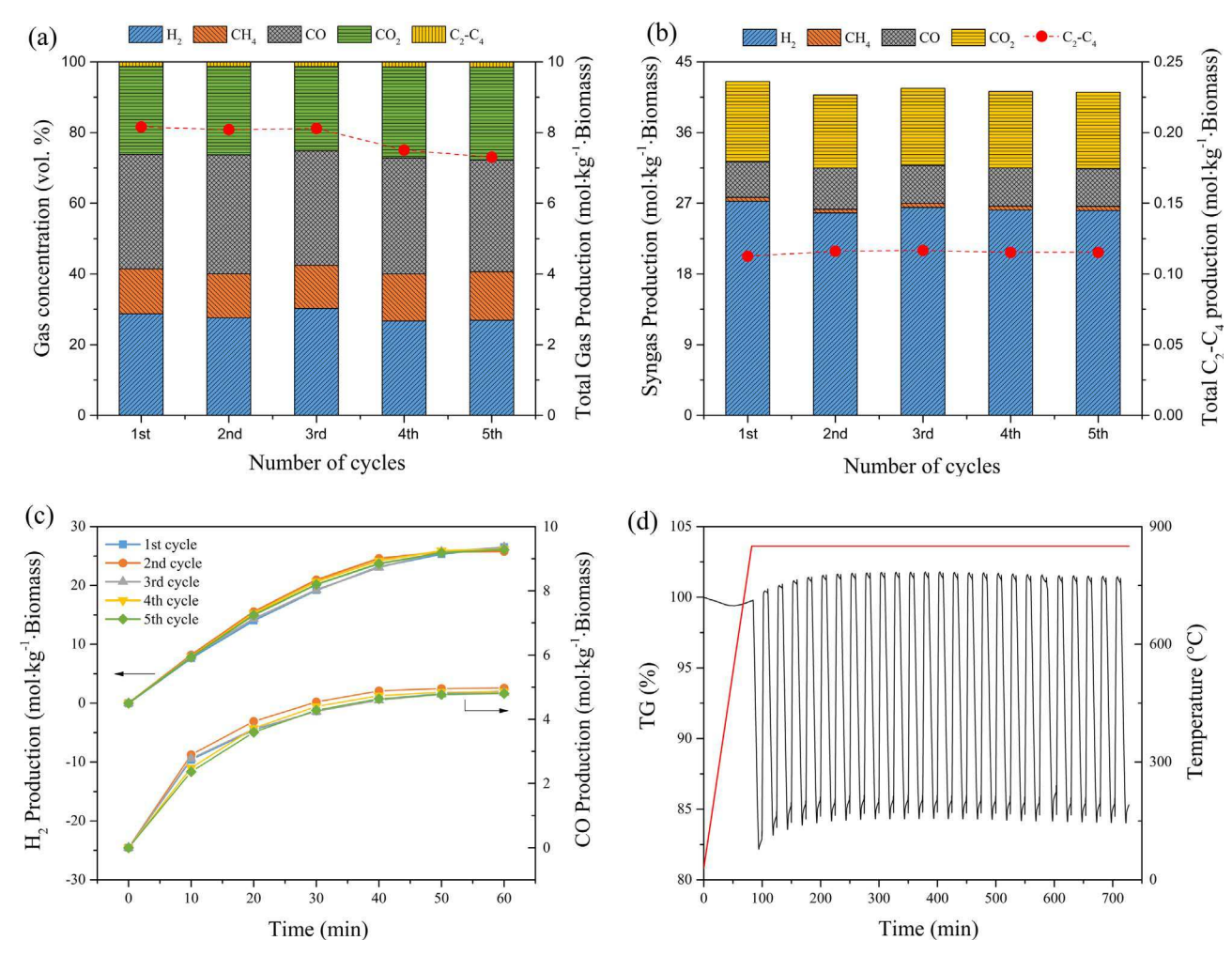


Fig. 8. Cyclic stability over 5 cycles of the $Ca_2Fe_2O_5$ catalyst for pine wood gasification with the N_2 flow rate of 30 mL/min, water injection rate of 0.10 mL/min, temperature of 850 °C, and gasification time of 60 min during (a) pyrolysis, (b) gasification, (c) H_2 and G yields, and (d) 20 cyclic simulated syngas reduction and G oxidation results using TGA.

steam biochar reaction (secondary):
$$C + 2H_2 O \rightarrow CO_2 + 2H_2$$
 (R11)

water gas shift:
$$CO + H_2 O \rightarrow CO_2 + H_2$$
 (R12)

steam methane reforming:
$$CH_4 + H_2 O \rightarrow CO + 3H_2$$
 (R13)

Boulouard reaction:
$$C + CO_2 \rightarrow 2CO$$
 (R14)

methanation:
$$C+ 2H_2 \rightarrow CH_4$$
 (R15)

The reaction path is changed with the addition of the $Ca_2Fe_2O_5$ catalyst in many ways, including (1) the reduced $Ca_2Fe_2O_5$ ($CaO + Fe^0$) in the pyrolysis stage is oxidized by steam, resulting in a higher hydrogen concentration and yield; (2) the water gas reaction is the main reaction during steam gasification process with the generation of CO and H_2 . The oxidized catalyst ($Ca_2Fe_2O_5$) would also be reduced by the produced CO gas. Similarly, the resulting Fe^0 is also rapidly oxidized by steam to generate Fe^{3+} . Thus, the inner-looping gasification is formed and the biochar is continuously converted according to the abovementioned redox reaction. Most importantly, the formation of the catalyst remains unchanged which could be reused further in the outer-looping experiments.

Accordingly, an inner-looping redox gasification and an outer-looping biomass conversion are proposed to understand the associated reaction mechanism as seen in Fig. 11. The inner looping gasification process is composed of two steps: (1) $\text{Ca}_2\text{Fe}_2\text{O}_5$ reduction with CO and Fe oxidation with H_2O under the existence of CaO (regeneration of $\text{Ca}_2\text{Fe}_2\text{O}_5$). Considering that the formation of $\text{Ca}_2\text{Fe}_2\text{O}_5$ remains unchanged after the catalytic pyrolysis and steam gasification process, the

outer looping is defined as cyclic pyrolysis and steam gasification. Supposing that x mol of CO gas was produced during steam gasification stage by primary steam biochar reaction, 3y mol of CO was reacted with $\text{Ca}_2\text{Fe}_2\text{O}_5$ catalyst, and z mol produced CO_2 was reacted with biochar, the reactions would be:

Primary steam biochar reaction:
$$xC + xH_2 O \rightarrow xCO + xH_2$$
 (R16)

$$Ca_2Fe_2O_5$$
 reduction with CO: $yCa_2Fe_2O_5 + 3yCO \rightarrow 2yCaO + 2yFe + 3yCO_2$ (R17)

Fe⁰ oxidation with steam: $2yFe + 2yCaO + 3yH_2 O \rightarrow yCa_2Fe_2O_5 + 3yH_2$ (R18)

Boulouard reaction:
$$zC + zCO_2 \rightarrow 2zCO$$
 (R19)

The net reaction of the inner-looping redox reaction would be:

$$3yCO + 3yH_2O \rightarrow 3yCO_2 + 3yH_2$$
 (R20)

The main net reaction during steam gasification stage is:

$$(x+z)C + (x+3y)H_2 O \rightarrow (x-3y+2z)CO + (x+3y)H_2 + (3y-z)CO_2$$
(R21

Hence, the addition of $Ca_2Fe_2O_5$ would promote the water gas shift reaction with Boudouard reaction promotion subsequently which accelerates the carbon conversion. The promotion degree depends on x, y, and z which are influenced by the factors of temperature, water injection rate, gasification time, and catalyst addition content.

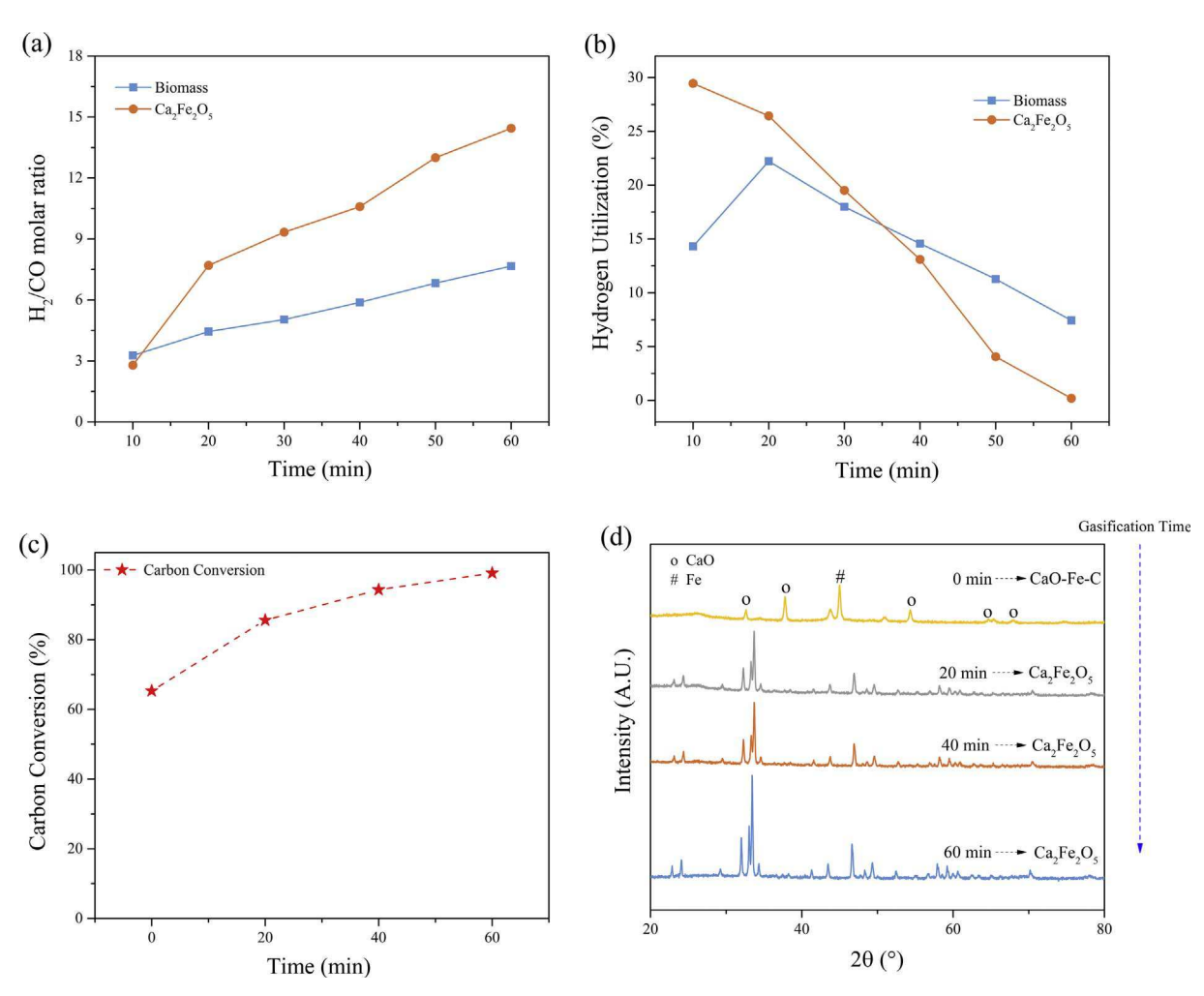


Fig. 9. The influence of reaction time on the (a) H_2/CO molar ratio, (b) hydrogen utilization, (c) carbon conversion, and (d) catalyst phase evolution from un-catalyzed or catalytic gasification of pine wood.

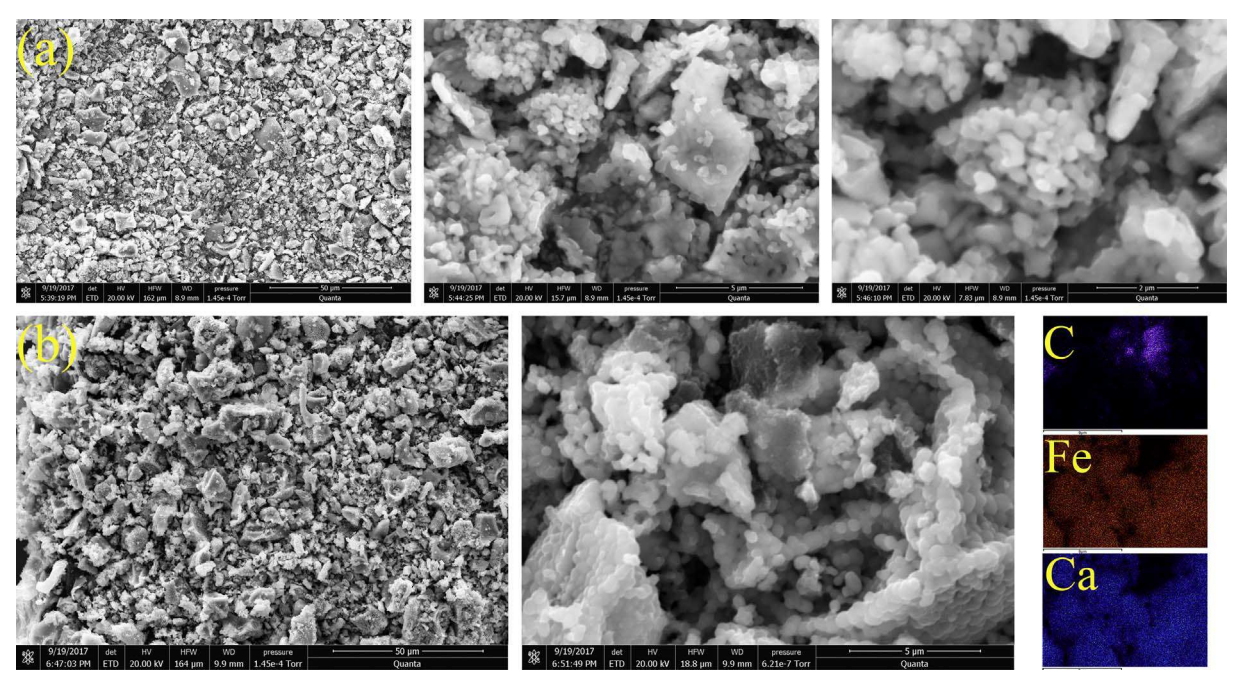


Fig. 10. SEM and EDS mapping results of fresh and reacted $Ca_2Fe_2O_5$ catalyst after once outer-looping experiment under the conditions of N_2 flow rate 30 mL/min, water injection rate 0.10 mL/min, temperature at 850 °C, and gasification time at 60 min.

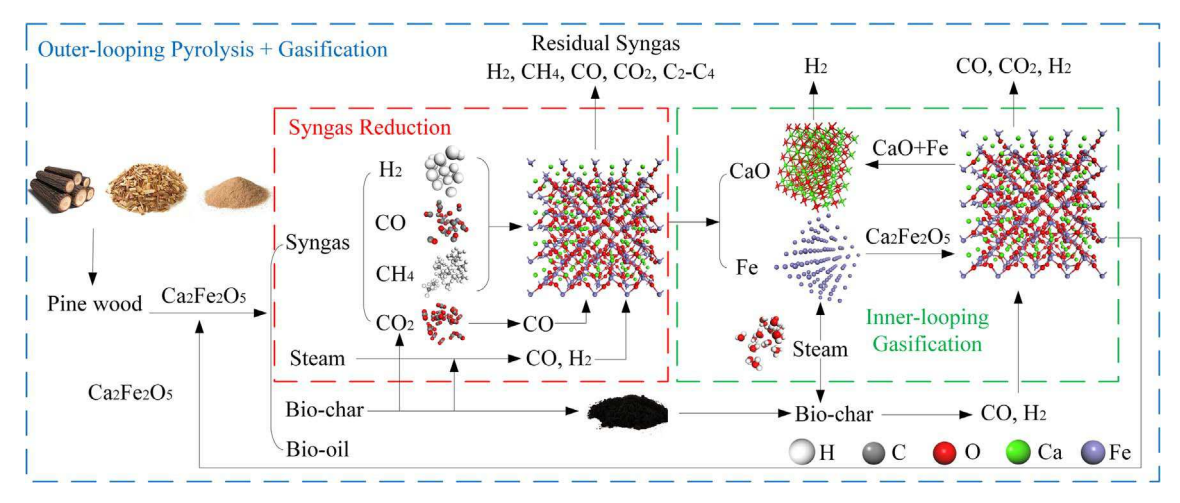


Fig. 11. Schematic of catalytic pine wood conversion (syngas reduction of pyrolysis stage and inner-looping promotion of steam gasification stage).

4. Conclusions

The new concepts integrated outer-looping biomass conversion and inner-looping redox gasification by using Ca₂Fe₂O₅ were proposed and confirmed. A number of findings result from the realization of the new concept. Firstly, the total gas production, tar cracking, and carbon conversion can be increased by 13.4%, 17.3%, and 11.7%, respectively with the addition of Ca₂Fe₂O₅. And the most significant increase in hydrogen production occurs at the initial 10 min of gasification, which improved the H₂ yields by 78.98%. Then, the effect of temperature, water injection rate, and catalyst load content were studied. Higher temperature and water injection rate are more favorable to hydrogen yields and carbon conversion. The operating conditions of temperature at 850 °C, water injection rate 0.10 mL/min, catalyst loading 10 wt.% are desired for the conversion of the tested pine wood. Moreover, Ca₂Fe₂O₅ was found to be stable after 20 cycles of syngas reduction and CO₂ oxidation. Finally, in catalytic pyrolysis, the resulting CO₂ and H₂O are beneficial to the tar and biochar conversion. The CaO generated from Ca₂Fe₂O₅ reduction promotes the tar cracking as well. In steam gasification, the inner-looping redox reaction of Ca₂Fe₂O₅ continuously enhances biochar gasification until a complete conversion of biochar. In summary, Ca₂Fe₂O₅ is a promising catalyst for large-scale biomass conversion application due to its continuous promoting mechanism and significant redox durability.

Acknowledgements

This work was supported by the National Natural Science Foundation of China (51576042) and National Science Foundation of US (1632899). The authors also appreciate the Fundamental Research Funds for the Central Universities, the Foundation of Graduate Creative Program of Jiangsu (KYLX16-0200), and the Scholarship Award granted to the first author by the Ministry of Education and China Scholarship Council for their support of the work.

Appendix A. Supplementary material

Supplementary data associated with this article can be found, in the online version, at http://dx.doi.org/10.1016/j.apenergy.2017.12.087.

References

- Sansaniwal S, Pal K, Rosen M, Tyagi S. Recent advances in the development of biomass gasification technology: a comprehensive review. Renew Sustain Energy Bev 2017;72:363–84
- [2] Li D, Tamura M, Nakagawa Y, Tomishige K. Metal catalysts for steam reforming of tar derived from the gasification of lignocellulosic biomass. Bioresource Technol 2015;178:53–64.

- [3] Udomchoke T, Wongsakulphasatch S, Kiatkittipong W, Arpornwichanop A, Khaodee W, Powell J, et al. Performance evaluation of sorption enhanced chemical-looping reforming for hydrogen production from biomass with modification of catalyst and sorbent regeneration. Chem Eng J 2016;303:338–47.
- [4] Kalinci Y, Hepbasli A, Dincer I. Biomass-based hydrogen production: a review and analysis. Int J Hydrogen Energy 2009;34:8799–817.
- [5] Chaiwatanodom P, Vivanpatarakij S, Assabumrungrat S. Thermodynamic analysis of biomass gasification with CO₂ recycle for synthesis gas production. Appl Energy 2014;114:10–7.
- [6] Srirangan K, Akawi L, Moo-Young M, Chou CP. Towards sustainable production of clean energy carriers from biomass resources. Appl Energy 2012;100:172–86.
- [7] Zhang S-P, Chen Z-Q, Cai Q-J, Ding D. The integrated process for hydrogen production from biomass: study on the catalytic conversion behavior of pyrolytic vapor in gas-solid simultaneous gasification process. Int J Hydrogen Energy 2016;41:6653–61.
- [8] Chen W-H, Lin B-J. Hydrogen and synthesis gas production from activated carbon and steam via reusing carbon dioxide. Appl Energy 2013;101:551–9.
- [9] Akbari-Emadabadi S, Rahimpour M, Hafizi A, Keshavarz P. Production of hydrogenrich syngas using Zr modified Ca-Co bifunctional catalyst-sorbent in chemical looping steam methane reforming. Appl Energy 2017;206:51–62.
- [10] Chen W-H, Lin B-J, Huang M-Y, Chang J-S. Thermochemical conversion of microalgal biomass into biofuels: a review. Bioresource Technol 2015;184:314–27.
- [11] Watanabe H, Li D, Nakagawa Y, Tomishige K, Watanabe MM. Catalytic gasification of oil-extracted residue biomass of *Botryococcus braunii*. Bioresource Technol 2015;191:452–9.
- [12] Zaini IN, Nurdiawati A, Aziz M. Cogeneration of power and H₂ by steam gasification and syngas chemical looping of macroalgae. Appl Energy 2017.
- [13] Han L, Wang Q, Luo Z, Rong N, Deng G. H₂ rich gas production via pressurized fluidized bed gasification of sawdust with in situ CO₂ capture. Appl Energy 2013;109:36–43.
- [14] Wu C, Wang L, Williams PT, Shi J, Huang J. Hydrogen production from biomass gasification with Ni/MCM-41 catalysts: influence of Ni content. Appl Catal B 2011:108:6–13.
- [15] Al-Rahbi AS, Williams PT. Hydrogen-rich syngas production and tar removal from biomass gasification using sacrificial tyre pyrolysis char. Appl Energy 2017;190:501–9
- [16] Chen F, Wu C, Dong L, Vassallo A, Williams PT, Huang J. Characteristics and catalytic properties of Ni/CaAlOx catalyst for hydrogen-enriched syngas production from pyrolysis-steam reforming of biomass sawdust. Appl Catal B 2016;183:168–75.
- [17] Moghadam RA, Yusup S, Azlina W, Nehzati S, Tavasoli A. Investigation on syngas production via biomass conversion through the integration of pyrolysis and air steam gasification processes. Energy Convers Manage 2014;87:670–5.
- [18] Díaz-Rey M, Cortés-Reyes M, Herrera C, Larrubia M, Amadeo N, Laborde M, et al. Hydrogen-rich gas production from algae-biomass by low temperature catalytic gasification. Catal Today 2015;257:177–84.
- [19] Richardson Y, Blin J, Volle G, Motuzas J, Julbe A. In situ generation of Ni metal nanoparticles as catalyst for H₂-rich syngas production from biomass gasification. Appl Catal A 2010;382:220–30.
- [20] Duman G, Uddin MA, Yanik J. Hydrogen production from algal biomass via steam gasification. Bioresource Technol 2014;166:24–30.
- [21] Baker EG, Mudge LK, Brown MD. Steam gasification of biomass with nickel secondary catalysts. Ind Eng Chem Res 1987;26:1335–9.
- [22] Harshini D, Yoon CW, Han J, Yoon SP, Nam SW, Lim T-H. Catalytic steam reforming of propane over Ni/LaAlO₃ catalysts: influence of preparation methods and OSC on activity and stability. Catal Lett 2012;142:205–12.
- [23] Chen G, Yao J, Liu J, Yan B, Shan R. Biomass to hydrogen-rich syngas via catalytic steam gasification of bio-oil/biochar slurry. Bioresource Technol 2015;198:108–14.
- [24] Sun Z, Xiang W, Chen S. Sorption enhanced coal gasification for hydrogen production using a synthesized CaO MgO-molecular sieve sorbent. Int J Hydrogen Energy 2016;41:17323–33.

[25] Zhang B, Zhang L, Yang Z, Yan Y, Pu G, Guo M. Hydrogen-rich gas production from wet biomass steam gasification with CaO/MgO. Int J Hydrogen Energy 2015;40:8816–23.

- [26] Sun Z, Toan S, Chen S, Xiang W, Fan M, Zhu M, et al. Biomass pyrolysis-gasification over Zr promoted CaO-HZSM-5 catalysts for hydrogen and bio-oil co-production with CO₂ capture. Int J Hydrogen Energy 2017.
- [27] Udomsirichakorn J, Basu P, Salam PA, Acharya B. Effect of CaO on tar reforming to hydrogen-enriched gas with in-process CO₂ capture in a bubbling fluidized bed biomass steam gasifier. Int J Hydrogen Energy 2013;38:14495–504.
- [28] Hirabayashi D, Sakai Y, Yoshikawa T, Mochizuki K, Kojima Y, Suzuki K, et al. Mössbauer characterization of calcium-ferrite oxides prepared by calcining Fe₂O₃ and CaO. ICAME 2005;2007:809–13.
- [29] Huang B-S, Chen H-Y, Chuang K-H, Yang R-X, Wey M-Y. Hydrogen production by biomass gasification in a fluidized-bed reactor promoted by an Fe/CaO catalyst. Int J Hydrogen Energy 2012;37:6511–8.
- [30] Zamboni I, Courson C, Kiennemann A. Fe-Ca interactions in Fe-based/CaO catalyst/ sorbent for CO₂ sorption and hydrogen production from toluene steam reforming. Appl Catal B 2017;203:154–65.
- [31] Ismail M, Liu W, Dunstan MT, Scott SA. Development and performance of iron based oxygen carriers containing calcium ferrites for chemical looping combustion and production of hydrogen. Int J Hydrogen Energy 2016;41:4073–84.
- [32] Ismail M, Liu W, Scott SA. The performance of Fe₂O₃-CaO oxygen carriers and the interaction of iron oxides with CaO during chemical looping combustion and H₂ production. Energy Proc 2014;63:87–97.
- [33] Grenier J-C, Pouchard M, Hagenmuller P. Vacancy ordering in oxygen-deficient perovskite-related ferrites. Ferrites Transit Elem Luminesc 1981:1–25.
- [34] Ross NL, Angel R, Seifert F. Compressibility of brownmillerite (Ca₂Fe₂O₅): effect of

- vacancies on the elastic properties of perovskites. Phys Earth Planet Interiors 2002;129:145–51.
- [35] Hirabayashi D, Yoshikawa T, Mochizuki K, Suzuki K, Sakai Y. Formation of brownmillerite type calcium ferrite (Ca₂Fe₂O₅) and catalytic properties in propylene combustion. Catal Lett 2006;110:269–74.
- [36] Isupova L, Tsybulya S, Kryukova G, Budneva A, Paukshtis E, Litvak G, et al. Mechanochemical synthesis and catalytic properties of the calcium ferrite Ca₂Fe₂O₅. Kinet Catal 2002;43:122–9.
- [37] Shin S, Hatakeyama Y, Ogawa K, Shimomura KY. Catalytic decomposition of NO over brownmillerite-like compounds, Ca₂Fe₂O₅ and Sr₂Fe₂O₅. Mater Res Bull 1979;14:133–6.
- [38] Sun Z, Chen S, Hu J, Chen A, Rony AH, Russell CK, et al. Ca₂Fe₂O₅: a promising oxygen carrier for CO/CH₄ conversion and almost-pure H₂ production with inherent CO₂ capture over a two-step chemical looping hydrogen generation process. Appl Energy 2018:211:431–42.
- [39] Chan MS, Liu W, Ismail M, Yang Y, Scott SA, Dennis JS. Improving hydrogen yields, and hydrogen: steam ratio in the chemical looping production of hydrogen using Ca₂Fe₂O₅. Chem Eng J 2016;296:406–11.
- [40] Shahbaz M, Inayat A, Patrick DO, Ammar M. The influence of catalysts in biomass steam gasification and catalytic potential of coal bottom ash in biomass steam gasification: a review. Renew Sustain Energy Rev 2017;73:468–76.
- [41] Chen G, Yao J, Yang H, Yan B, Chen H. Steam gasification of acid-hydrolysis biomass CAHR for clean syngas production. Bioresource Technol 2015;179:323–30.
- [42] Huang B-S, Chen H-Y, Kuo J-H, Chang C-H, Wey M-Y. Catalytic upgrading of syngas from fluidized bed air gasification of sawdust. Bioresource Technol 2012;110:670–5.